Indirect polarization alignment with points on the sky, the Hub Test

Richard Shurtleff *

May 19, 2021

Abstract

The alignment of transverse vectors on the sky, such as the polarization directions of electromagnetic radiation from astronomical sources, can be an interesting property of the sources themselves or of the intervening medium between source and detector. For many regions of the Milky Way the alignment of the polarization directions of starlight is evident. However evident visually, it is useful to have a numerical alignment function that can be used to judge the significance of the correlations. The test described here evaluates the tendency for aligned directions to focus on points in the sky, as well as correlations in their avoidance of points in the sky. The formulas needed to conduct the test are derived and two illustrative examples are provided. In one sample from the Milky Way, the polarization directions from starlight are seen to converge far from the sample and, for another sample, a set of quasars with polarized radio emissions, the convergence occurs close to the sample.

Keywords: Polarization ; Alignment ; Large scale structure

1 Introduction

Partially polarized starlight traces Galactic Magnetic fields, helping to understand Galactic structure [1, 2] and to inform the physics of the contaminating dust [3, 4] that obscures more distant objects of interest, such as quasi stellar objects (QSOs). The linear polarization of electromagnetic emissions of QSOs [5, 6] provides, for example, evidence of correlations between polarization directions and large scale structure. [7, 8] Detailed maps of the polarized cosmic microwave background radiation provide another subject for alignment studies. [9]

At all of these scales and for a variety of reasons, the alignment of a set of sources can be an interesting property. The test described in this paper provides a quantitative geometric basis for judging alignment.

Existing tests, for example, the 'S' and 'Z' tests, Ref. [5,6,10], collect the polarization directions together, rating how well position angles agree. These tests are blind to samples with well-correlated polarization directions when those directions focus down on a point that is close to the sources. Only samples with nearly parallel position angles and with necessarily distant convergence can be detected.

The alternate test described here extends the polarization directions around the Celestial Sphere, forming a set of geodesics, *a.k.a.* great circles. Those great circles converge in places on the sphere and diverge at other places. The locations of best convergence and the locations of greatest divergence are "hubs", a name associated with important transportation centers which are places where great circle travel routes converge.

*affiliation and mailing address: Department of Sciences, Wentworth Institute of Technology, 550 Huntington Avenue, Boston, MA, USA, 02115, orcid.org/0000-0001-5920-759X, e-mail: shurtleffr@wit.edu, momentummatrix@yahoo.com

A circle of sources each with polarization directions aimed radially, like the spokes of a bicycle wheel, are arguably well correlated, but do not favor a single position angle and would not be considered well aligned by direct comparison tests like the S and Z tests. Less severe is the case with the polarization directions converging on a hub that is very close to the sources on the sky. Parallax requires the polarization directions to depend on each source's location. Again, the S and Z tests, looking for equal polarization directions, would not detect such an alignment. A set of sources that exhibit such a pattern is discussed in Sec. 4.

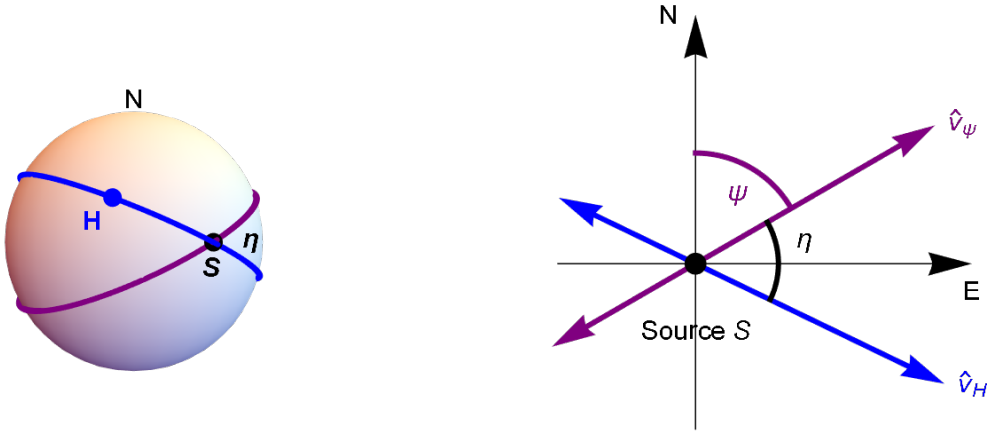

Figure 1: (Color online) *A source S of polarized EM radiation and a point H are plotted on the Celestial sphere.* (a) The source S and point H determine a great circle. The polarization direction is tangent to a second great circle. The angle η is the acute angle between the two circles at S. (b) In the plane tangent to the Celestial sphere at S, the polarization position angle PPA is an angle ψ measured clockwise from North with East to the right. The angle η quantifies how well the polarization direction $\hat{v}_\psi$ aligns with the direction $\hat{v}_H$ toward H from S.

In general, astronomical sources are candidates for an alignment test if there is an observed asymmetry such as linear polarization or some other feature like a jet or an axis of rotation. The alignment of linear polarization directions is discussed here, but the test is easily adapted to other features.

At each point H on the Celestial sphere, given a position angle ψ, the angle η in Fig. 1 is the basis for an alignment angle function $\eta(H)$. For a sample with many sources, the angles η from the sources can be averaged and that gives an alignment angle function $\bar{\eta}(H)$ for the sample.

At points H where the function $\bar{\eta}(H)$ is small, the great circles in the direction of the polarizations converge. Conversely, points H where $\bar{\eta}(H)$ is high indicate divergence. The extremes are located at "hubs", alignment hubs $H_{\rm min}$ and $-H_{\rm min}$ where the function $\bar{\eta}(H)$ takes its minimum value and avoidance hubs $H_{\rm max}$ and $-H_{\rm max}$ where the alignment angle is at a maximum.

The discussion in Sec. 2 includes the derivation of formulas needed to calculate the alignment angle function $\bar{\eta}(H)$ for a given sample. The function can be mapped on the Celestial Sphere to give a visual display. See Figs. 5 and 7 in Sec. 4.

The 'significance' of an alignment result means the fraction of random runs that would give the same or a better result. Hence, significance can be estimated by evaluating the results of many runs with random

polarization data. The process and the significance formulas are presented in Sec. 3. Similarly, to gauge the effects of experimental uncertainty, one runs many sets of data, each set slightly off the catalog values in a way that reflects measurement uncertainties. This topic is also discussed in Sec. 3.

Two very significantly aligned samples are analyzed with the Hub test in Sec. 4. The first sample analyzes data found in two catalogs of polarized starlight, Heiles 2000 and Berdyugin 2014, [11,12]. The second sample analyzes data from Pelgrims 2014, which is identifies QSO radio sources in the large JVAS/CLASS 8.4Ghz catalog Jackson 2007. [10, 13]

The first sample discussed in Sec. 4 aligns with a point $H_{\rm min}$ that is far from the sources, while the second sample's alignment hub $H_{\rm min}$ is very close to the sample. Thus the two cases show the extremes of possible alignments and the type of information retrieved by the Hub test.

2 The Hub Test

The data required to run the Hub test consists of the locations of 'sources' S_i, each with a 'polarization position angle' PPA ψ_i.

The basic quantity calculated with the Hub Test is the "alignment angle" η of a polarization direction and the direction to a point H on the Celestial Sphere. As shown in Fig. 1, the "alignment angle" η separates the tangents to two Great Circles where they cross at S. One Great Circle moves away from S along the polarization direction and the other Great Circle connects S and H. In (b) one sees that the alignment angle η is measured at the source in the tangent plane of the source.

One should note some basic geometry. The angle η is the same for all points H' on the great circle connecting S and H. However, the angle η is undefined where either H or $-H$ coincides with the source S or $-S$. Aside from the few points where it cannot be defined, the angle η has the same value at $-H$ as it does at H. Also, all great circles through H contain the diametrically opposite point $-H$. Only H and $-H$ are common to all the Great Circles through H. It follows that, as a function of H, the alignment angle $\eta(H)$ is symmetric across diameters, $\eta(H) = \eta(-H)$. Now for some math.

Given a point on the unit sphere with known longitude, latitude angles, one can determine the radial unit vector from the origin to the point in rectangular coordinates (x, y, z). One has

$$\hat{\mathbf{r}} = (x, y, z) = (\cos\alpha\cos\delta,\, \sin\alpha\cos\delta,\, \sin\delta)\ . \tag{1}$$

The formula works whether we are in Equatorial Coordinates with (Right Ascension,Declination) = (RA,dec) = (α, δ) or Galactic coordinates with galactic longitude and latitude (l, b) replacing (α, δ) in (1).

Writing the same equations with the different notations of two different coordinate systems must not be confused with the problem of transforming coordinates from one system to the other. In this and the following sections, we continue to write formulas with the (α, δ) longitude and latitude notation for the Equatorial Coordinate System, while recognizing the same equations are valid with the (l, b) longitude and latitude of the Galactic Coordinate System.

In Cartesian coordinates, the unit vectors, $\hat{\mathbf{v}}_{\rm N}$ and $\hat{\mathbf{v}}_{\rm E}$, in the direction of local North and local East in the plane tangent to the sphere at S are given by

$$\hat{\mathbf{v}}_{\rm N} = (-\cos\alpha\sin\delta,\, -\sin\alpha\sin\delta,\, \cos\delta)\ ;\ \hat{\mathbf{v}}_{\rm E} = (-\sin\alpha,\, \cos\alpha, 0)\ . \tag{2}$$

The three vectors $\hat{\mathbf{r}}_S$, $\hat{\mathbf{v}}_{\rm N}$, and $\hat{\mathbf{v}}_{\rm E}$ form an orthonormal set.

All vectors in the tangent plane at S, see Fig. 1(b), are linear combinations of local North $\hat{\mathbf{v}}_{\rm N}$ and local East $\hat{\mathbf{v}}_{\rm E}$. Both the unit vector $\hat{\mathbf{v}}_\psi$ in the direction of ψ and its cross product with the radial unit vector $\hat{\mathbf{r}}_S$

are vectors in the tangent plane at S and we have

$$\hat{\mathbf{v}}_\psi = \cos\psi\,\hat{\mathbf{v}}_{\rm N} + \sin\psi\,\hat{\mathbf{v}}_{\rm E} \quad ; \quad \hat{\mathbf{n}}_{S\times\psi} = \hat{\mathbf{r}}_S \times \hat{\mathbf{v}}_\psi = \sin\psi\,\hat{\mathbf{v}}_{\rm N} - \cos\psi\,\hat{\mathbf{v}}_{\rm E}\,, \tag{3}$$

where the cross product $\hat{\mathbf{n}}_{S\times\psi}$ is perpendicular to $\hat{\mathbf{v}}_\psi$. One can show that the three vectors $\hat{\mathbf{r}}_S$, $\hat{\mathbf{v}}_\psi$, $\hat{\mathbf{n}}_{S\times\psi}$ form an orthonormal set.

Let the point H on the sphere in Fig. 1 be located at (RA,dec) $= (\alpha_H, \delta_H)$. The point H must not be S or $-S$. Clearly, the Great Circle containing H and S lies in the plane spanned by $\hat{\mathbf{r}}_H$ and $\hat{\mathbf{r}}_S$. Since the unit vector tangent to the great circle at the source S, $\hat{\mathbf{v}}_H$, lies in the plane of the great circle, the tangent vector $\hat{\mathbf{v}}_H$ must be a linear combination of $\hat{\mathbf{r}}_H$ and $\hat{\mathbf{r}}_S$.

Since $\hat{\mathbf{v}}_H$ is tangent to the sphere at S, we know that $\hat{\mathbf{v}}_H$ is perpendicular to $\hat{\mathbf{r}}_S$. By applying the Gram-Schmidt process to $\hat{\mathbf{r}}_H$ and $\hat{\mathbf{r}}_S$, we get $\hat{\mathbf{v}}_H$ from $\hat{\mathbf{r}}_H$ by subtracting off the part of $\hat{\mathbf{r}}_H$ that is parallel to $\hat{\mathbf{r}}_S$. The result is

$$\hat{\mathbf{v}}_H = \frac{\hat{\mathbf{r}}_H - (\hat{\mathbf{r}}_S \cdot \hat{\mathbf{r}}_H)\hat{\mathbf{r}}_S}{\mid \hat{\mathbf{r}}_H - (\hat{\mathbf{r}}_S \cdot \hat{\mathbf{r}}_H)\hat{\mathbf{r}}_S \mid}\,, \tag{4}$$

where the dot product $\hat{\mathbf{r}}_S \cdot \hat{\mathbf{r}}_H = \cos\theta$ is the cosine of the angle between unit vectors $\hat{\mathbf{r}}_H$ and $\hat{\mathbf{r}}_S$. Since the denominator is the length of the vector in the numerator, the result is a unit vector.

The fundamental quantity in the Hub test is the alignment angle η between the polarization direction ψ and the direction toward the point H, as illustrated in Fig. 1. One can determine η from the dot product of unit vectors $\hat{\mathbf{v}}_H$ and $\hat{\mathbf{v}}_\psi$,

$$\cos\eta = \mid \hat{\mathbf{v}}_H \cdot \hat{\mathbf{v}}_\psi \mid\ . \tag{5}$$

We want the acute angle between the two directions. Since the absolute value makes $\cos\eta$ non-negative, the alignment angle η can be acute, restricted to the range $0° \le \eta \le 90°$.

The angle η can be chosen to be acute because the electric field polarization direction and the tangent to the great circle from S to H are not oriented: the electric field oscillates back and forth along $\pm\hat{\mathbf{v}}_\psi$ and both directions $\pm\hat{\mathbf{v}}_H$ connect S to H.

Consider the unit vector $\hat{\mathbf{n}}_{S\times H}$ that is perpendicular to the plane of the great circle through H and S,

$$\hat{\mathbf{n}}_{S\times H} = \frac{\hat{\mathbf{r}}_S \times \hat{\mathbf{r}}_H}{\mid \hat{\mathbf{r}}_S \times \hat{\mathbf{r}}_H \mid}\,. \tag{6}$$

By the properties of cross products, the unit vector $\hat{\mathbf{n}}_{S\times H}$ is perpendicular to both $\hat{\mathbf{r}}_S$ and $\hat{\mathbf{r}}_H$. Thus $\hat{\mathbf{n}}_{S\times H}$ is in the plane tangent to the sphere at S. By (4), $\hat{\mathbf{v}}_H$ is a linear combination of $\hat{\mathbf{r}}_S$ and $\hat{\mathbf{r}}_H$, it follows that $\hat{\mathbf{n}}_{S\times H}$ is perpendicular to $\hat{\mathbf{v}}_H$. Thus the vector $\hat{\mathbf{n}}_{S\times H}$ lies in the plane tangent to the sphere at S in a direction perpendicular to $\hat{\mathbf{v}}_H$. To avoid overcrowding, the vector $\hat{\mathbf{n}}_{S\times H}$ is not drawn in Fig. 1(b).

In the plane tangent to the sphere at S, the perpendicular directions $\hat{\mathbf{n}}_{S\times H} \perp \hat{\mathbf{v}}_H$ and $\hat{\mathbf{n}}_{S\times\psi} \perp \hat{\mathbf{v}}_\psi$ differ by the same angle as $\hat{\mathbf{v}}_H$ and $\hat{\mathbf{v}}_\psi$. Thus, as an alternate to (5) one can also determine η from

$$\cos\eta = \mid \hat{\mathbf{n}}_{S\times\psi} \cdot \hat{\mathbf{n}}_{S\times H} \mid\ . \tag{7}$$

Whether one uses (5) or (7), the formulas (1) through (7) allow the alignment angle η to be calculated given the PPA ψ and the locations (α_S, δ_S) and (α_H, δ_H) of the source S and point H on the sphere.

To be useful, the Hub test must be applied to a sample, a collection of many sources S_i, $i \in 1, ..., N$, where N is the number of sources. Each source S_i has a given location on the sphere, (α_i, δ_i), that is part of the original data. Each source has a polarization direction determined by a polarization position angle PPA denoted ψ_i. Then, for each point H on the sphere, there is an alignment angle η_{iH}, as pictured in Fig. 1 and calculated with either Eq. (5) or (7), but now for each of N sources.

For almost all points H on the sphere, one can define an average alignment angle function $\bar{\eta}(H)$ representing how well aligned with H, on average, are the polarization directions of the collection of sources S_i. Let the function $\bar{\eta}(H)$ be defined as

$$\bar{\eta}(H) = \bar{\eta}(\alpha, \delta) = \frac{1}{N} \sum_i \eta_{iH} \,, \tag{8}$$

where (RA,dec) = (α, δ) is the location of H. To be more precise, this is the arithmetic mean. Plots of the function $\bar{\eta}(\alpha, \delta)$ for the samples in Sec. 4 are displayed in Figs. 5 and 7.

Since all the alignment angles η_{iH} are acute angles, as noted after Eq. (5), it follows that their average, the function $\bar{\eta}(H)$, is also an acute angle, $0° \leq \bar{\eta}(H) \leq 90°$.

The function $\bar{\eta}(H)$ cannot be defined where H or $-H$ is coincident with any of the sources, $\pm H \neq \pm S_i$. From Fig. 1, when S and H are the same point, infinitely many great circles 'connect' them, so there is no well defined angle η. There is a corresponding effect in the formulas; $\hat{\mathbf{v}}_H$ in (4) is indeterminate, 0/0, when $\hat{\mathbf{r}}_H$ and $\hat{\mathbf{r}}_S$ coincide.

As noted earlier, the angle η in Fig. 1 is a diametrically symmetric function of H, so the average of many ηs, the alignment function $\bar{\eta}(H)$ in (8) obeys

$$\bar{\eta}(H) = \bar{\eta}(-H) \,, \tag{9}$$

showing that the alignment function $\bar{\eta}(H)$ is symmetric across diameters.

The maximum and minimum values of $\bar{\eta}(H)$ have special meanings. The Hub test provides numerical results $\bar{\eta}_{\rm min}$ and $\bar{\eta}_{\rm max}$ that can be used to judge how strongly the sources' polarization directions are correlated with $H_{\rm min}$ and $H_{\rm max}$. The locations of the max and min points on the sphere, $\pm H_{\rm min}$ and $\pm H_{\rm max}$, that the polarization directions tend to point towards or away from are also potentially useful information determined by the test.

Once one has determined the smallest alignment angle $\bar{\eta}_{\rm min}$ and the largest avoidance angle $\bar{\eta}_{\rm max}$ for the observed data, it is important to know how likely it is that random polarization directions would have returned equivalent or better results. The problem of significance is treated next.

3 Significance Level and Uncertainty

How do we know if the alignment is significant? What is the likelihood that sources with random PPA polarization angles would produce a lower $\bar{\eta}_{\rm min}$ or a higher $\bar{\eta}_{\rm max}$?

To find out, we make many random runs, repeating the process in Sec. 2, but with sources that have randomly polarized PPA data. The random run results produce raw probability distributions that can be approximated with functions. Functions that fit the distributions of random run results can be used to estimate the significance of observed alignments.

It is found that useful parameters include the angular extent of a sample as well as the number of sources in the sample. Runs with a small number of sources are found to be more likely to have lower $\bar{\eta}_{\rm min}$ and higher $\bar{\eta}_{\rm max}$ when compared to runs with large numbers of sources. The dependence on sample extent is less pronounced than the dependence on the number of sources.

A random run starts by choosing the number N of sources and the radius ρ of the sample region. Then choose N sources at random locations in the region and assign random PPA ψ polarization angles to each. The alignment angle η_{iH} between the ith source and the grid point H is calculated as in Sec. 2. The average (arithmetic mean) $\bar{\eta}_H$ of the N alignment angles η_{iH} at each grid point H is calculated. The largest and

smallest average alignment angles, $\bar{\eta}_{\rm min}$ and $\bar{\eta}_{\rm max}$, are determined as well as the hub locations $H_{\rm min}$ and $H_{\rm max}$ where the extreme angles occur. The locations of the sources, their PPA angles ψ, the location $H_{\rm min}$, the smallest average alignment angle $\bar{\eta}_{\rm min}$, the location $H_{\rm max}$, and the largest average alignment angle $\bar{\eta}_{\rm max}$ are collected and stored. That completes the random run.

The sources were confined to regions of radii $\rho = \{0°, 5°, 12°, 24°, 48°, 90°\}$. By diametrical symmetry, the 90° region effectively covers the entire sphere. The number N of sources in each region were assigned to be $N = \{8, 16, 32, 64, 128, 181, 256, 512\}$. All cases were run $R = 2000$ times.

One should not interpret the results for a region with radius $\rho = 0°$ as results for an unpolarized source. An unpolarized or circularly polarized source has its linear polarization randomly or uniformly cycling though all directions perpendicular to the line of sight. Here we have N definite and unchanging polarization directions from independent sources that happen to be located in a tiny region.

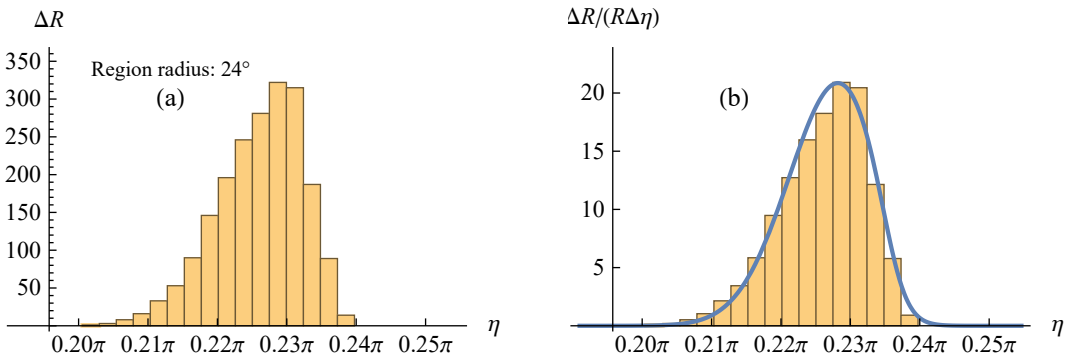

Figure 2: (Color online) $R = 2000$ *runs for* $N = 181$ *sources with random polarization PPA* ψ. For each run, the sources were assigned random polarization directions ψ. The best alignment angle $\bar{\eta}_{\rm min}$ for each of the R runs was collected and the results analyzed. In (a), the histogram of $\bar{\eta}_{\rm min}$ plots the number of runs ΔR in each bin of width $\Delta\bar{\eta} = 0.0025\pi$ radians. The total number of runs is the sum of the bar heights, $R = \sum \Delta R$. Thus, by dividing by $R\Delta\bar{\eta}$, the sum of the areas of the bars in (b) is unity, an approximation to the probability distribution. In the foreground is the distribution, (10), that fits the data, slightly steeper on the $\eta = \pi/4 = 0.25\pi$ high side than on the low side.

The random runs use a $2° \times 2°$ grid, or mesh. Since location is irrelevant for the random runs, the sources are confined to a single region for most of the runs, a region centered near the grid point at (RA,dec) $= (71.9°, 59.4°)$. Sources are chosen at random from the grid points within the region and moved slightly off-grid to avoid resonances. However, for point-like regions with null radii, $\rho = 0°$, the math was simpler with the sources at the North pole.

In symbols, for $R(N)$ runs with a given number of sources N, there are a total of $R(N)$ values of $\bar{\eta}_{\rm min}$ and $\bar{\eta}_{\rm max}$. By counting the number $\Delta R_i^{\rm min}$ of values of $\bar{\eta}_{\rm min}$ that are found in an interval $\Delta\eta$ centered on η_i, one obtains a histogram, the collection $\{\eta_i, \Delta R_i^{\rm min}\}$. Since the total number of runs is the sum, $R = \sum \Delta R_i$, the fraction of random results $\bar{\eta}_{\rm min}$ that are in the ith bin is $\Delta R_i/R$. The fraction $\Delta R_i/R$ approximates the probability of finding $\bar{\eta}_{\rm min}$ with a value in the $i^{\rm th}$ bin.

As an example, the histogram for random runs in a 24° radius region with $N = 181$ sources is presented in Fig. 2(a). In part (b), the histogram is rescaled so that its total area is unity, just like a probability

distribution.

By trying various formulas, we find one that fits the random data well. We choose

$$P^{\min}(\eta) = \frac{1.220}{\sigma\sqrt{2\pi}} \left(1 + e^{4(\frac{\eta-\eta_0}{\sigma} - 1)}\right)^{-1} e^{-\frac{1}{2}\left(\frac{\eta-\eta_0}{\sigma}\right)^2} \quad , \tag{10}$$

where $1.220 = \sqrt{2\pi}/\int [e^{-y^2/2}/(1 + e^{4(y-1)})]dy$. Since $P(\eta_0 + 0.706\sigma) = P(\eta_0 - 1.018\sigma) = e^{-1/2}P(\eta_0)$, the 'width' is the quantity $0.706\sigma + 1.018\sigma = 1.72\sigma$. The label "min" in $P^{\min}(\eta)$ indicates "alignment."

The probability distribution $P(\eta)$ is the product of a normal distribution with a unit step, an 'S-curve'. The S-curve is unity for small η and vanishes for large η, with a transition on the $\pi/4$ side of the histogram. The S-curve makes the $\eta = \pi/4$ side of the distribution steeper. See Fig. 2. Making the $\pi/4$ side steeper pushes probability to the other side. However the step function nears unity on the side of interest, the small η side opposite the $\eta = \pi/4$ side. Since the step function is unity, the side of interest behaves as a normal distribution with mean η_0 and half-width σ, but with an altered normalization constant, 1.220 in place of 1.000 .

To judge avoidance, the maximum angles $\bar{\eta}_{\max}$ of the random runs were collected. All such angles exceed $\pi/4$; one has $\bar{\eta}_{\max} > \pi/4$. Similar to the alignment cases, the side of an avoidance histogram toward $\eta = \pi/4$ is steeper than the far side toward $\eta = \pi/2$. Making the necessary adjustment to the formula, two sign changes compared with (10), the random results can be fit with an avoidance probability distribution $P^{\max}(\eta)$ given by

$$P^{\max}(\eta) = \frac{1.220}{\sigma\sqrt{2\pi}} \left(1 + e^{-4(\frac{\eta-\eta_0}{\sigma} + 1)}\right)^{-1} e^{-\frac{1}{2}\left(\frac{\eta-\eta_0}{\sigma}\right)^2} \quad . \tag{11}$$

As with alignment, the side of interest, the high side toward $\eta = \pi/2$ is where the step function becomes unity and the function is a normal distribution but with a scaling factor of 1.220 in place of 1.000 .

For both alignment and avoidance, the likelihood that a random result $\bar{\eta}$ is in an interval $\delta\eta$ centered on η is approximated by $P(\eta)\delta\eta$. Choose $P^{\min}(\eta)$ for alignment and $P^{\max}(\eta)$ for avoidance.

By fitting probability distributions (10) and (11) to histograms for $R(N)$ random runs with N sources in a region of radius ρ and $N = \{8, 16, 32, 64, 128, 181, 256, 512\}$, one finds a mean value $\eta_0(N)$ and a half-width $\sigma(N)$ for each N. It turns out that the various $\eta_0(N)$ and $\sigma(N)$ are well described by simple functions of $\sqrt{N}$,

$$\eta_0^{\min}(N) = \frac{\pi}{4} - \frac{c_1}{\left(\sqrt{N}\right)^{a_1}} \approx \frac{\pi}{4} - \frac{1}{\sqrt{N}} \quad ; \quad \sigma^{\min}(N) = \frac{c_2}{4\left(\sqrt{N}\right)^{a_2}} \approx \frac{1}{4\sqrt{N}} \tag{12}$$

$$\eta_0^{\max}(N) = \frac{\pi}{4} + \frac{c_1}{\left(\sqrt{N}\right)^{a_1}} \approx \frac{\pi}{4} + \frac{1}{\sqrt{N}} \quad ; \quad \sigma^{\max}(N) = \frac{c_2}{4\left(\sqrt{N}\right)^{a_2}} \approx \frac{1}{4\sqrt{N}} \quad ,$$

where the parameters c_i and a_i for $\eta_0^{\min}$ and $\eta_0^{\max}$ have values near unity, depending on the radius ρ of the region. See Table 1. The simpler expressions in (12) apply when the parameters a_i and c_i are equal to one.

Note that, for random runs at $\rho = 5^\circ$ and especially for $\rho = 0^\circ$ with any given number N of sources, the alignment and avoidance angles approach the midway value $\pi/4$ much closer than they do for larger regions. See Table 1, where c_1 is noticeably smaller for $\rho = 5^\circ$ and 0° than it is for regions with larger radii ρ.

With random data, the sum on the right in (8) is a sum of random numbers constrained to the interval $[0, \pi/2]$ with a mean value of $\pi/4$. One can show that the dependence on $\sqrt{N}$ of $\eta_0^{\min}(N)$ and $\eta_0^{\max}(N)$ in

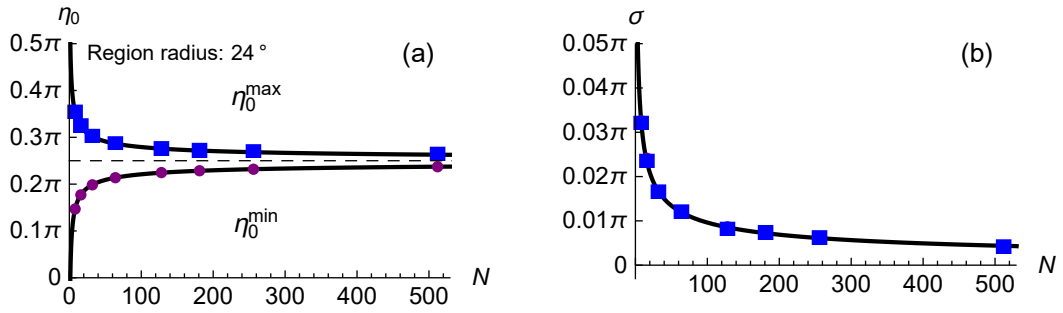

Figure 3: (Color online) *For $\rho = 24°$ radius regions, the mean η_0 and half-width σ parameters for random runs as functions of the number of sources N in (12) and Table 1.* (a) Note that avoidance (max) and alignment (min) are symmetric about the dashed line at the angle $0.25\pi = 45°$. (b) Since, for $\rho > 5°$, all of the parameters in Table 1 are roughly unity, $c_i, a_i \approx 1$, the half-widths σ are about $1/(4\sqrt{N})$, which, by (12), is a quarter of the separation of the η_0 curves in (a) from the dashed centerline $\eta_0 = \pi/4$.

(12) can be made plausible by adapting random walk ideas. [14] In random walk language, at each point H on the sphere, except at sources or opposite sources, define the "distance" function D_N by

$$D_N \equiv N\left(\bar{\eta}(H) - \frac{\pi}{4}\right) = \sum_i^N \left(\eta_{iH} - \frac{\pi}{4}\right) = D_{N-1} + s \quad , \tag{13}$$

where we use (8) and where s is a 'step', the change that gives D_N from D_{N-1}.

From Fig. 1, with a random polarization direction ψ for the N^{th} source, the alignment angle η is as likely to be greater than $\pi/4$ as it is to be less than $\pi/4$. Thus each step $s = (\eta_{iH} - \pi/4)$ is as likely to be positive as it is to be negative. By repeating over many trials, we infer that the average step s would vanish, $\langle s\rangle = 0$.

However, the square of s, *i.e.* s^2, is always positive or zero. Let us assume that the average of s^2 is a constant, $\langle s^2\rangle = d^2$, while maintaining $\langle s\rangle = 0$. Then the average of D_N^2 increases with N,

$$\langle D_N^2\rangle = \langle (D_{N-1} + s)^2\rangle = \langle D_{N-1}^2\rangle + \langle s^2\rangle = \langle D_1^2\rangle + (N-1)d^2 = Nd^2 \quad , \tag{14}$$

where we assume that $\langle D_1^2\rangle = d^2$. The root-mean-square value $D_N^{\text{rms}} \equiv \sqrt{\langle D_N^2\rangle} = \pm d\sqrt{N}$ and, by (13), we have

$$\bar{\eta}^{\text{rms}}(H) = \frac{\pi}{4} \pm \frac{d}{\sqrt{N}} \quad , \tag{15}$$

which is much like (12).

To make (15) equivalent to (12), the extreme value of the constant d would need to be one radian. This means that the added source contributes an amount $d^2 = \langle (\eta_{NH} - \pi/4)^2\rangle = 1$ to $\langle D_N^2\rangle$ in (14), on average for max avoidance or best alignment. Justifying that conclusion is a more complicated problem than I want to consider here. So, let us settle for having shown that the dependence of $\eta_0^{\min}(N)$ and $\eta_0^{\max}(N)$ on $\sqrt{N}$ in (12) is made plausible by the coincidence of (12) and (15).

Fig. 3 plots the functions in (12) and the means $\eta_0(N)$ and the half-widths $\sigma(N)$ from random runs with sources in a $\rho = 24°$ region.

Region Radius ρ	$c_1^{\min}$	$a_1^{\min}$	$c_2^{\min}$	$a_2^{\min}$
90°	0.9423 ± 0.0050	1.0046 ± 0.0036	1.061 ± 0.026	0.954 ± 0.016
48°	0.9505 ± 0.0079	1.0156 ± 0.0057	1.166 ± 0.016	0.9956 ± 0.0095
24°	0.9235 ± 0.0024	1.0069 ± 0.0018	1.127 ± 0.022	0.964 ± 0.013
12°	0.8912 ± 0.0034	1.0054 ± 0.0026	1.238 ± 0.039	1.021 ± 0.021
5°	0.8363 ± 0.0035	1.0088 ± 0.0028	1.076 ± 0.030	0.940 ± 0.019
0°	0.5031 ± 0.0059	1.0153 ± 0.0080	1.522 ± 0.052	1.053 ± 0.024
Region Radius	$c_1^{\max}$	$a_1^{\max}$	$c_2^{\max}$	$a_2^{\max}$
90°	0.9441 ± 0.0061	1.0055 ± 0.0044	1.000 ± 0.038	0.931 ± 0.025
48°	0.9572 ± 0.0063	1.0165 ± 0.0045	1.090 ± 0.026	0.958 ± 0.016
24°	0.927 ± 0.011	1.0068 ± 0.0079	1.101 ± 0.019	0.964 ± 0.011
12°	0.9049 ± 0.0069	1.0090 ± 0.0052	1.228 ± 0.039	1.018 ± 0.022
5°	0.8424 ± 0.0038	1.0062 ± 0.0031	1.168 ± 0.022	0.992 ± 0.013
0°	0.4982 ± 0.0058	1.0093 ± 0.0080	1.543 ± 0.057	1.060 ± 0.025

Table 1: *Parameters c_i and a_i, i = 1,2 in (12) for regions with various radii ρ.* By the symmetry across diameters, the region with a radius of 90° covers the whole sphere. The parameters c_i for $\rho > 5°$ and a_i for any ρ are close to unity, some equal to one within the plus/minus standard error.

Let us use Fig. 3 to visualize the probability distributions in (10), (11), and (12). The bulk of the most likely alignment angles $\bar{\eta}_{\min}$ and avoidance angles $\bar{\eta}_{\max}$ extend vertically a little above and a little below the η_0 curves drawn in (a). The half-widths σ in (b) are a quarter of the separation, *i.e.* $1/\sqrt{N} = \mid \pi/4 - \eta_0 \mid$, in (a) between the angle $\pi/4$ to the η_0 curves. So the max and min avoidance and alignment angles $\bar{\eta}$ of a given random run will most likely fall in two bands centered on the η_0 curves, bands whose half-widths σ are about a quarter of the separation from $\pi/4$ to the η_0 curves. With that pictured, we leave random runs and return to observations.

Given an 'observed' alignment angle $\bar{\eta}^{\rm obs}_{\min}$, *i.e.* one that is calculated from observed polarizations, there is a chance that randomly directed polarizations can produce an equal or smaller alignment angle. The "significance" S of a particular $\bar{\eta}^{\rm obs}_{\min}$ is defined to be the likelihood that random runs will show better alignment than indicated by the observed angle.

Similarly, there is a likelihood that the avoidance angle $\bar{\eta}^{\rm obs}_{\max}$ could be less than the result of some random run. We therefore define two significances $S^{\min}(\bar{\eta}^{\rm obs}_{\min})$ and $S^{\max}(\bar{\eta}^{\rm obs}_{\max})$, one for alignment and one for avoidance.

Given the approximations $P(\eta)$ in (10) and (11) to the probability distributions, the significance of an alignment or avoidance angle $\bar{\eta}^{\rm obs}$ is the integral from/to infinity,

$$S^{\min}(\bar{\eta}^{\rm obs}_{\min}) = \int_{-\infty}^{\bar{\eta}^{\rm obs}_{\min}} P^{\min}(\eta){\rm d}\eta \quad ; \quad S^{\max}(\bar{\eta}^{\rm obs}_{\max}) = \int_{\bar{\eta}^{\rm obs}_{\max}}^{\infty} P^{\max}(\eta){\rm d}\eta \quad . \tag{16}$$

The significance formula for an observed min alignment angle $\bar{\eta}^{\rm obs}_{\min}$ is the fraction of random runs that would yield better alignment, *i.e.* a smaller alignment angle $\bar{\eta}_{\min}$. Similarly, the significance formula for an observed max avoidance angle $\bar{\eta}^{\rm obs}_{\max}$ in (16) indicates the likelihood that random runs would produce larger avoidance angles than the angle $\bar{\eta}^{\rm obs}_{\max}$ that is calculated from observed data.

The distributions in (10) and (11) approximate the scaled histograms of the results of random runs as in Fig. 2. Note that the distributions have nonzero values for any real η, positive or negative, while alignment

and avoidance angles $\bar{\eta}$ are confined to a finite interval, *i.e.* they are nonnegative acute angles $0° \leq \eta \leq 90°$. So, there might be a problem.

Probabilities and significances are meaningless for PPA angles that are negative, $\bar{\eta} < 0°$, or larger than a right angle, $\bar{\eta} > 90° = \pi/2$ rad. With only slight differences due to the parameters c_i and a_i, by (16), we have $S_N^{\min}(0) \approx S_N^{\max}(\pi/2)$, which means that the significance of the disallowed angles smaller than 0 and larger than $90° = \pi/2$ are about the same. For $N = 4$ sources in 24° radius regions, one calculates $S_{N=4}^{\min}(0) \approx S_{N=4}^{\max}(\pi/2) = 0.014$, which is more than 1% and is not negligible when determining significance. Upon increasing number of sources to $N = 7$, one finds that $S_{N=7}^{\min}(0) \approx S_{N=7}^{\max}(\pi/2) = 4 \times 10^{-5}$ or 0.004%. That may be considered negligible. For the examples discussed in the next section, only regions with seven or more sources are considered.

4 Two applications of the Hub test

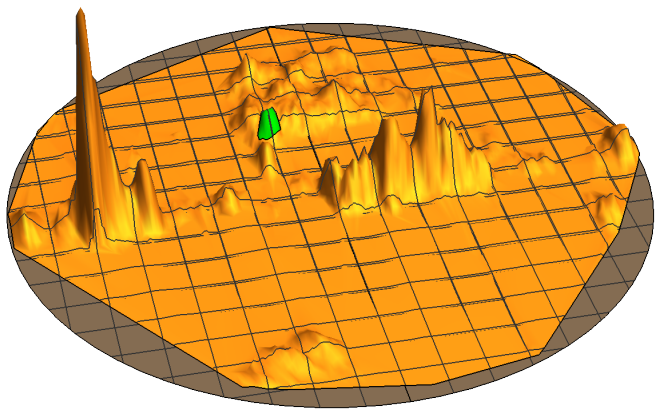

Figure 4: *Survey of polarized Galactic starlight.* The function $h(l, b)$ is plotted, where $h = -\log_{10}(S)$ and S is the significance of the alignment for 5° radius regions centered on grid points. Only very significant regions are shown in orange, $h = -\log S > 2$. The largest peaks occur along the Galactic Disk. The hill shaded Green is located off-Disk and Northeast of the Galactic Center and is composed of 35 of the 5° radius regions. These 35 regions combine to make the 99-star sample considered in the text. The most significant of the 35 regions has a height $h = -\log S \approx 30$, meaning that it is better aligned than all but one in 10^{30} randomly directed regions. (Galactic coordinates; $(+180°, 0°)$ on the left; an Aitoff plot; Color online.)

In this section, two samples are discussed. One has the polarization directions narrowly constrained and the alignment hubs are far from the sources. The second sample has polarizations directions pointing to a hub located near the sources and parallax forces the polarization directions to have a wide range of position angles.

The first sample consists of Milky Way stars. To get a rough idea of the alignment of the polarized starlight, we conduct a survey. The polarized starlight data is taken from two catalogs, Heiles 2000 and Berdyugin 2014, [11, 12]. Each grid point on a $2^\circ \times 2^\circ$ mesh serves as the center of a 5°-radius region. The regions are populated with stars from the catalogs. Requiring at least 7 stars per region ensures the formulas of Sec. 3 will be sufficiently accurate.

A kind of "topographical" map of the Milky Way Galaxy is presented in Fig. 4. Fig. 4 shows the topography of significance for polarized Galactic starlight, arranged so that higher elevations indicate more significant alignment. Significance is difficult to plot, so the altitudes h in Fig. 4 are the negative log of significance, $h = -\log_{10}(S)$. The highest peak on the left tops off at $-\log S \approx 270$ and that means the significance $S \approx 10^{-270}$, essentially nil.

It should be noted that the topographical map for the significance of avoidance is nearly identical to the topographical map for alignment, *i.e.* both look like Fig. 4. It may be that the collections of small regions of the Galaxy with significantly aligned polarized starlight imply that these are regions where the starlight passes through essentially the same interstellar medium, giving a somewhat uniform result. Polarized starlight in regions that do not align significantly may pass through incoherent ISM.

The first sample consists of one of the lower hills Northeast of the Galactic Center, shaded green in Fig. 4. The sample has 99 stars. The 99 stars are shared by the 5°-radius regions that have centers (l, b) with $17^\circ \leq l \leq 34^\circ$, $23^\circ \leq b \leq 35^\circ$ and $b < 23^\circ - 1.5(l - 36^\circ)$. The last inequality separates the sample from an adjacent hill. All of these 5°-radius regions have $S^{\min} \leq 10^{-9}$, so, in Fig. 4 their altitude h is at least 9, $h \geq 9$.

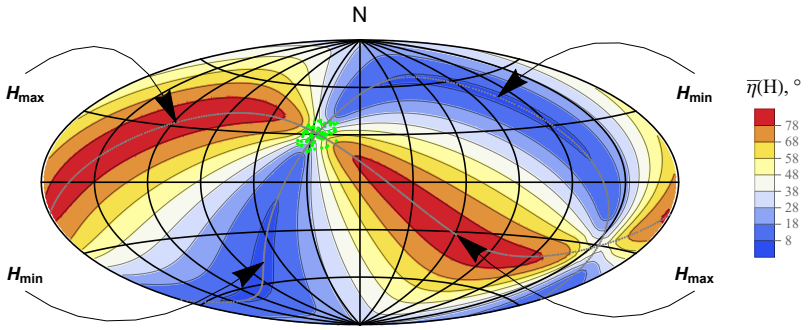

Figure 5: *The alignment function $\bar{\eta}(H)$, Eq. 8.* The sources are located at the green dots. To guide the eye, two Great Circles are drawn, one through the sources' center and the avoidance hubs $\pm H_{\max}$, while the other connects the sources' center with the alignment hubs $\pm H_{\min}$. The two Great Circles are shaded Gray and, within experimental uncertainty, they are perpendicular where they cross at the sources' center. (Galactic coordinates with $(+180^\circ, 0^\circ)$ on the left and $(-180^\circ, 0^\circ)$ on the right, an Aitoff plot, Color online.)

Sample	Coordinates	N	$\bar{\eta}_{\min}$	$H_{\min}$	Significance of $\bar{\eta}_{\min}$
Stars	Galactic	99	$7.25° \pm 0.27°$	$(77.9°, -50.6°) \pm (6.9°, 4.0°)$	$< 10^{-71} \approx 0$
QSOs	Equatorial	27	$21.77° \pm 0.88°$	$(9.7°, 1.5°) \pm (2.4°, 2.6°)$	$1.2^{+3.0}_{-0.9} \times 10^{-5}$

Table 2: *Alignment metrics.*

Sample	Coordinates	N	$\bar{\eta}_{\max}$	$H_{\max}$	Significance of $\bar{\eta}_{\max}$
Stars	Galactic	99	$82.80° \pm 0.27°.$	$(120.9°, 31.0°) \pm (4.8°, 2.3°)$	$< 10^{-71} \approx 0$
QSOs	Equatorial	27	$66.07° \pm 0.96°$	$(144.°, -25.°) \pm (20.°, 14.°)$	$2.0^{+3.6}_{-1.4} \times 10^{-4}$

Table 3: *Avoidance metrics.*

Combining these 5°-radius regions into a single sample makes a combined sample that is even more significantly aligned, combined, the significance becomes $S^{\min} \approx 10^{-71}$. The significance and other metrics for the sample can be found on the first line in Tables 2 and 3.

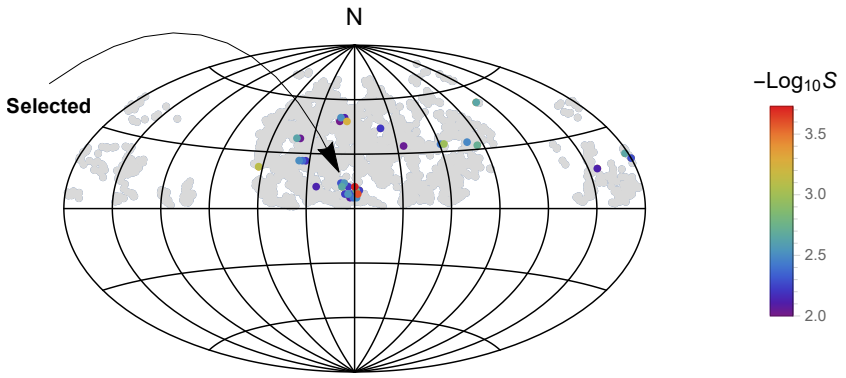

Figure 6: *Survey of polarized radio QSOs.* The 1450 QSOs were grouped into 5° radius regions centered on grid points. Those regions having at least 7 QSOs are plotted as gray dots at the central grid point. Just 35 regions showed very significant alignment, i.e. $S \leq 0.01 = 10^{-2}$, or, equivalently, $-\log_{10} S \geq 2.0$, and these are plotted as color dots. The indicated clump of 14 regions was selected for the analysis. There are 27 QSOs in the combined area of the 14 regions. (Equatorial coordinates centered on $(\alpha, \delta) = (180°, 0°)$, with $(360°, 0°)$ on the right, an Aitoff plot, Color online.)

The angular separation of the furthest star from the sample center is 11.84°. Accordingly, we choose the statistics constants a_i and c_i for sources confined to regions with radii $\rho = 12°$ in Table 1. By (12), one finds that, with randomly directed polarizations, the expected smallest alignment angle $\bar{\eta}_{\min}$ is $\bar{\eta}_{\min}^{\text{Random}\psi}$

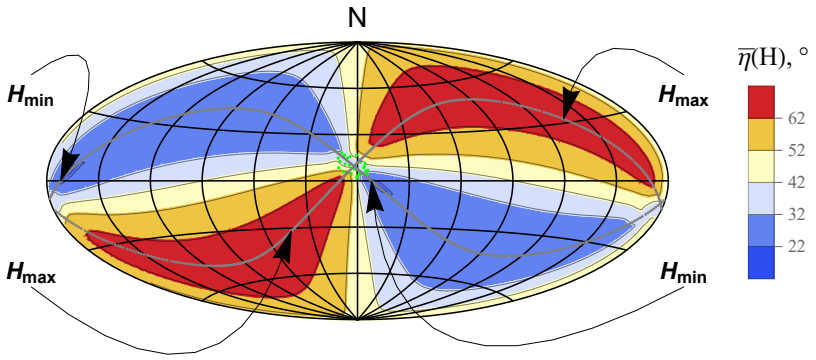

Figure 7: *The alignment function $\bar{\eta}(H)$ for the QSO sample.* The sources are located at the green dots. As in Fig. 4, the two Great Circles are perpendicular where they meet. Unlike the Star sample in Fig. 5, the QSO sample has an alignment hub $H_{\min}$ that is so close to the sources that parallax is important. (Equatorial coordinates with $(0°, 0°)$ on the left and $(360°, 0°)$ on the right, an Aitoff plot, Color online.)

$= \eta_0^{\min} \pm \sigma^{\min} = 40.0° \pm 1.7°$, (Random ψ). The expected largest avoidance angle $\bar{\eta}_{\max}$ is $\bar{\eta}_{\max}^{\text{Random }\psi} = \eta_0^{\max} \pm \sigma^{\max} = 50.1° \pm 1.7°$, (Random ψ).

By applying Eq. (8) to the observed data for the sample, one finds the alignment function $\bar{\eta}(H)$ depicted in Fig. 5. The smallest alignment angle $\bar{\eta}_{\min}$ is about 7° and the largest avoidance angle $\bar{\eta}_{\max}$ is 83°. Both are about 19σs from the mean results, 40° and 50°, with randomly directed polarizations. One can reasonably conclude that the alignment and avoidance correlations are not due to chance.

In Fig. 5, one sees that the closest alignment hub $H_{\min}$ sits in a convergence region on the sphere well away from the sources. The angular separation is 89° from the sample's center, which is almost as far away as possible. By the symmetry across diameters, anything beyond 90° would force $-H_{\min}$ to be closer than $H_{\min}$.

This sample, with its hubs located so far away, is a prototype for samples whose sources have nearly equal polarization directions, making their alignment evident. The alignment is evident from the position angle histogram in Fig. 8(a).

To test the agreement of the Hub test with the S and Z tests, we calculate the position angle PA for the direction from the center of the region in Fig. 7 to the hub $H_{\min}$. We find that the PA is 151°. The value sits midway in the clump of observed PPA ψs Fig. 8(a). The agreement confirms that the Hub test and the S and Z tests can yield similar conclusions about whether or not polarization directions align.

At the other extreme, a sample's sources can converge on a hub $H_{\min}$ that is very close to the sample. In such a case the polarization directions from different parts of the sample are different. The position angle histogram shows a spread out distribution of position angles, even if the polarization directions all aimed toward a single point.

As an example, we consider a sample of Quasi-Stellar Objects, QSOs. The data is found in Pelgrims 2014, [10], a catalog of 1450 QSOs that have been identified as QSOs in the earlier JVAS/CLASS 8.4Ghz catalog Jackson 2007 that has 12700 records. [13] These are sources of linearly polarized radio emissions.

As above with starlight from Galactic sources, we first conduct a survey. The 1450 extra-galactic radio sources populate 5°-radius regions each centered on a grid point of a whole-sky $2° \times 2°$ grid. The sample

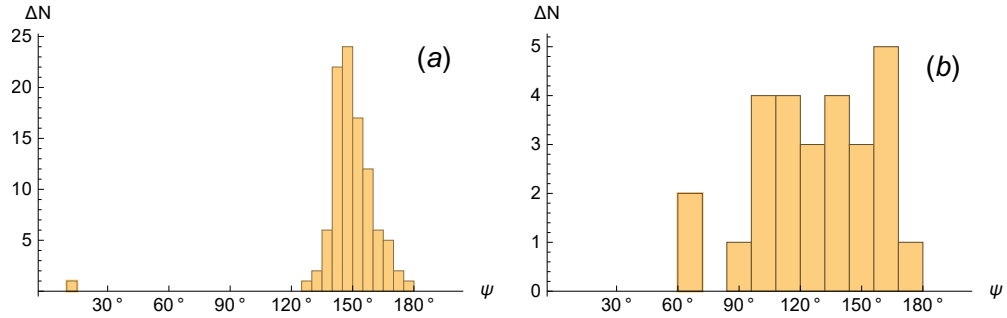

Figure 8: *Histograms of the polarization position angles ψ for (a) Stars and (b) QSOs.* (a) Stars. The position angles of the polarization directions cluster around $\psi = 151°$, which is the position angle to the alignment hub $H_{\rm min}$ in Fig. 5. Alignment is clear and the hub is far from the sources. (b) For the QSO sample, the position angle from the sample's center toward the hub $H_{\rm min}$ is 133°. But here, parallax produces many position angles and alignment is not clear from the ψ histogram. However, the Hub test looks for convergence and has no trouble detecting the alignment of the polarization directions in the sample.

studied here combines the QSO sources in a cluster of 14 very significantly aligned 5°-radius regions near the North Galactic Pole. The most significantly aligned 5°-radius region is one of the regions in the cluster.

The sample of partially polarized QSOs consists of 27 sources. With formulas from Sec. 2, one can calculate the alignment function $\bar{\eta}(H)$ for this sample. The function is depicted in Fig. 7. Metrics of the alignment can be found in Tables 2 and 3. The significance of the smallest alignment angle $\bar{\eta}_{\rm min}$ puts the 27-source sample better aligned than 8 random samples in a million.

In Fig. 7, the great circles in the polarization directions converge at the alignment hub $H_{\rm min}$ which is just 14° from the sample center. That means the polarization directions are not equal, but spread out in value so that they can point to $H_{\rm min}$ from any location in the sample, *i.e.* parallax. The histogram of the position angles in Fig. 8(b) shows that the PAs are evenly spread out over about 60°. This type of well-correlated alignment would be difficult to detect with tests that look for a cluster of PAs centered on a unique value.

5 Conclusions

The extreme case of alignment of the polarized starlight evident in Figs. 5 has parallel polarization directions converging on a distant hub $H_{\rm min}$. The perpendiculars to the polarization directions likewise clump and the avoidance hub $H_{\rm max}$ is likewise distant. Distant hubs, far from the sources, characterize one extreme of highly significant alignment.

The other extreme of alignment occurs when the polarization directions focus down on a point near the sources. There is parallax. When the point of best alignment is close to the sources, the polarization directions are correlated, but they are not parallel, since they tend to point in different directions from different locations in the sample.

The samples also differ by the significance of the alignments. The survey of QSO alignment tendencies finds correlated alignments that are much weaker than polarized Galactic starlight. The most significantly aligned 5°-radius QSO region is better aligned than one in 5000 randomly polarized similar samples. That

level of significance makes it unlikely that it is due to chance. Yet, with the starlight survey, there are many regions in Fig. 4 that are better aligned than millions of randomly polarized samples.

Finally, one can see that there is much more interest in the literature devoted to alignment as opposed to avoidance, perhaps because avoidance is not measured. The notion of 'avoidance' is measurable with the Hub test. The surveys reveal samples of starlight and QSOs that significantly avoid their hub points $H_{\max}$, while their alignments are lax. Perhaps highly significant avoidance may be an indicator of different polarization mechanisms than those indicated by alignment. The topic needs further investigation.

Acknowledgments. My thanks to V. Pelgrims for sending me the JVAS1450 catalog that gives redshifts and identifies the QSOs among the unclassified radio sources in the JVAS/CLASS 8.4-GHz catalog. Both V. Pelgrims and N. Ridge helpfully suggested including more content than appeared in earlier versions. This research did not receive any specific grant from funding agencies in the public, commercial, or not-for-profit sectors. Conflicts of interest: none.

References

[1] J. L. Han, R. N. Manchester, W. van Straten, and P. Demorest. Pulsar rotation measures and large-scale magnetic field reversals in the galactic disk. *The Astrophysical Journal Supplement Series*, 234(1):11, jan 2018.

[2] Ian W. Stephens, Leslie W. Looney, C. Darren Dowell, John E. Vaillancourt, and Konstantinos Tassis. The galactic magnetic fields effect in star-forming regions. *The Astrophysical Journal*, 728(2):99, jan 2011.

[3] A. Lazarian and Thiem Hoang. Alignment and rotational disruption of dust. *The Astrophysical Journal*, 908(1):12, feb 2021.

[4] Guillet, V., Fanciullo, L., Verstraete, L., Boulanger, F., Jones, A. P., Miville-Deschênes, M.-A., Ysard, N., Levrier, F., and Alves, M. Dust models compatible with planck intensity and polarization data in translucent lines of sight. *A&A*, 610:A16, 2018.

[5] D. Hutsemekers. Evidence for very large-scale coherent orientations of quasar polarization vectors. *Astronomy and Astrophysics*, 332:410–428, April 1998.

[6] P. Jain, G. Narain, and S. Sarala. Large-scale alignment of optical polarizations from distant QSOs using coordinate-invariant statistics. *MNRAS*, 347:394–402, January 2004.

[7] Damien Hutsemkers, Lorraine Braibant, Vincent Pelgrims, and Dominique Sluse. Alignment of quasar polarizations with large-scale structures. *Astron. Astrophys.*, 572:A18, 2014.

[8] Vincent Pelgrims and Damien Hutsemkers. Evidence for the alignment of quasar radio polarizations with large quasar group axes. *Astron. Astrophys.*, 590:A53, 2016.

[9] Planck Collaboration. Planck 2018 results: XII. galactic astrophysics using polarized dust emission. *Astronomy and Astrophysics*, 641, September 2020.

[10] V. Pelgrims and J. R. Cudell. A new analysis of quasar polarization alignments. *MNRAS*, 442:1239–1248, August 2014.

[11] Carl Heiles. 9286 Stars: An Agglomeration of Stellar Polarization Catalogs. *Astron. J.*, 119(2):923–927, February 2000.

[12] Berdyugin, A., Piirola, V., and Teerikorpi, P. Interstellar polarization at high galactic latitudes from distant stars - viii. patterns related to the local dust and gas shells from observations of 3600 stars. *A&A*, 561:A24, 2014.

[13] N. Jackson, R. A. Battye, I. W. A. Browne, S. Joshi, T. W. B. Muxlow, and P. N. Wilkinson. A survey of polarization in the JVAS/CLASS flat-spectrum radio source surveys - I. The data and catalogue production. *MNRAS*, 376:371–377, March 2007.

[14] Emanuel Parzen. *Modern probability theory and its applications.* A Wiley publication in mathematical statistics. Wiley, New York, 1960.